

# Theoretical guidelines to create and tune electric skyrmions

M.A.P. Gonçalves<sup>1</sup>, Carlos Escorihuela-Sayalero<sup>1</sup>, Pablo García-Fernández<sup>2</sup>, Javier Junquera<sup>2</sup> and Jorge Íñiguez<sup>1</sup>

<sup>1</sup>*Materials Research and Technology Department, Luxembourg Institute of Science and Technology (LIST), Avenue des Hauts-Fourneaux 5, L-4362 Esch/Alzette, Luxembourg*

<sup>2</sup>*Departamento de Ciencias de la Tierra y Física de la Materia Condensada, Universidad de Cantabria, Cantabria Campus Internacional, Avenida de los Castros s/n, 39005 Santander, Spain*

arXiv:1806.01617v1 [cond-mat.mtrl-sci] 5 Jun 2018

Magnetic skyrmions are mesmerizing spin textures with peculiar topological and dynamical properties, typically the product of competing interactions in ferromagnets, and with great technological potential [1–5]. Researchers have long wondered whether analogous electric skyrmions might exist in ferroelectrics, maybe featuring novel behaviors and possibilities for electric and mechanical control. The results thus far are modest, though: an electric equivalent of the most typical magnetic skyrmion (which would rely on a counterpart of the Dzyaloshinskii-Moriya interaction) seems all but impossible; further, the exotic ferroelectric orders observed or predicted to date [6–8] rely on very specific nano-structures (composites, superlattices), which limits the generality and properties (e.g., mobility) of the possible associated skyrmions. Here we propose an original approach to write electric skyrmions in simple ferroelectric lattices in a customary manner. Our second-principles simulations [9] of columnar ferroelectric nano-domains, in prototype compound  $\text{PbTiO}_3$ , show that it is possible to harness the Bloch-type internal structure of the domain wall [10] and hence create a genuine skyrmion. We check that the object thus obtained displays the usual skyrmion-defining features; further, it also presents unusual ones, including a symmetry-breaking skyrmion-skyrmion transition driven by strain, various types of topological transformations induced by external fields and temperature, and potentially very small sizes. Our results suggest countless possibilities for creating and manipulating electric textures with non-trivial topologies, using standard experimental tools and materials, effectively inaugurating the field of electric skyrmions.

Magnetic skyrmions (MSKs) are spin structures with unusual topological, dynamical and response properties [1–5]. Skyrmions are characterized by a non-zero integer topological charge

$$Q = \int q(x, y) dx dy, \quad (1)$$

where the Pontryagin density  $q(x, y)$  is given by

$$q = \frac{1}{4\pi} \mathbf{u} \cdot (\partial_x \mathbf{u} \times \partial_y \mathbf{u}). \quad (2)$$

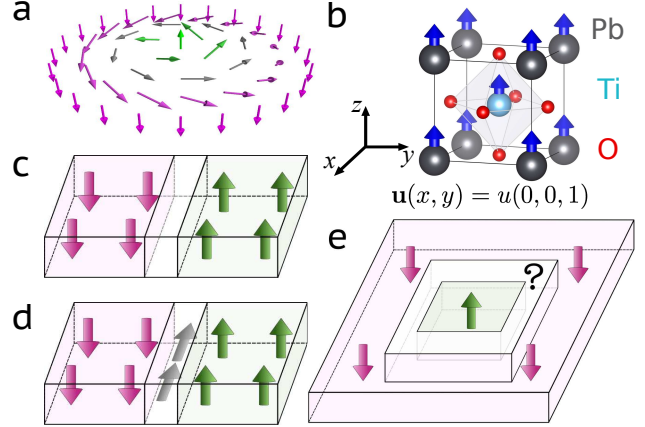


FIG. 1. Sketches of (a) a typical Bloch-like MSK; (b) the unit cell of  $\text{PbTiO}_3$ , where arrows mark the displacements yielding a local polarization  $P_z$  or, equivalently, a vector field  $\mathbf{u} \parallel (0, 0, 1)$ ; structure of the  $180^\circ$  FE DW of PTO at high (c) and low (d)  $T$ , as predicted in Ref. 10; (e) ND within a matrix of opposite polarization investigated in this work.

Here,  $\mathbf{u} = \mathbf{u}(x, y)$  is a vector field that describes the spin order in the  $xy$  plane in an idealized continuum limit. The MSK sketched in Fig. 1a has  $Q = 1$ ; in contrast, the most usual spin arrangements (e.g., ferromagnetic, spin spirals) all present  $Q = 0$ . Beyond their fundamental interest, skyrmions hold definite technological promise, e.g. for racetrack memories [11, 12], and constitute a very exciting field in today’s condensed-matter physics and materials science.

MSKs are typically found in ferromagnets featuring competing interactions whose combined action, often in presence of thermal activation and external fields, results in non-trivial spin arrangements. Ferroelectrics (FEs) form another well-known family of ferroics where competing couplings abound [13, 14]. Hence, one would expect to find in FEs an electric analogue of MSKs, with electric dipoles in place of spins. However, electric skyrmions (ESKs) remain elusive.

The apparent lack of ESKs may be partly due to existing differences between spins and electric dipoles. For example, it is proving all but impossible to find an electric analogue of the Dzyaloshinskii-Moriya interaction, which favors non-collinear spin arrangements and is a common ingredient to obtain small MSKs. More importantly, electric dipoles are the result of local symmetrywise-polar lattice distortions whose amplitude can vary continuously

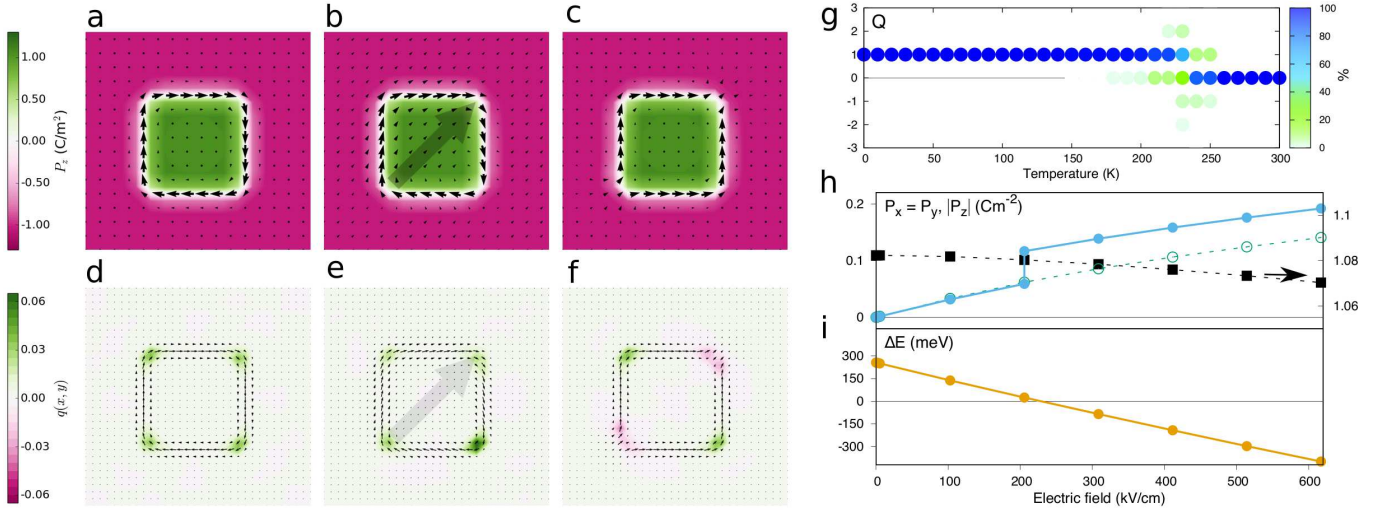


FIG. 2. Calculated polarization [(a)–(c)] and Pontryagin density [(d)–(f)] maps for: our ND within a matrix in its ESK ground state [(a) & (d)], the same ND-ESK subject to an in-plane electric field along (1,1) [(b) & (e)]; the field is indicated by a shadowed arrow, and the NDW-polar state stabilized for large enough field values [(c) & (f)]. In (a)–(c), the color scale gives the out-of-plane  $P_z$  component, while the arrows correspond to the in-plane  $P_x$  and  $P_y$ . Panel (g): Probability distribution for  $Q$  as a function of  $T$ . Panel (h): polarization as a function of in-plane electric field; black filled squares give  $|P_z|$  as obtained at the middle of either matrix or ND (right vertical axis; the results for matrix and ND are essentially identical, and very close to those for a monodomain state); blue filled circles give the  $P_x = P_y$  components (left axis), obtained from a supercell average and normalized to the supercell volume; green open circles give the monodomain result for  $P_x = P_y$ . Panel (i): Energy difference  $\Delta E = E_{\text{NDW-polar}} - E_{\text{ND-ESK}}$  between the NDW-polar and ND-ESK states as obtained in a  $16 \times 16 \times 1$  supercell. Note that the ND-ESK and NDW-polar solutions are (meta)stable in the whole field range here considered. In panels (b) and (e) we show the ND-ESK solution at 500 kV/cm, to better visualize the shift of the ESK center; in panels (c) and (f) we show the NDW-polar solution at zero field.

(Fig. 1b). Hence, instead of accommodating competing interactions by forming skyrmions, electric dipoles can just vanish, while spins (typically) cannot.

Nevertheless, recent studies suggest where to find interesting dipole textures, e.g., mediating nucleation [15] or switching [16] of FE domains, or induced by defects [17]. Further, vortex-like dipole structures and bubble domains have been observed in heterostructures that combine FE ( $\text{PbTiO}_3$  or  $\text{PbZr}_{1-x}\text{Ti}_x\text{O}_3$ ) and paraelectric ( $\text{SrTiO}_3$  or STO) layers [8, 18–21], suggesting that exotic orders may occur under appropriate electrostatic boundary conditions. Electrostatics is also responsible for the ESKs predicted to occur in FE ( $\text{BaTiO}_3$ ) pillars inside a paraelectric (STO) matrix [6, 7, 22]. While encouraging, these examples rely on complex artificial nano-structures, which limits the generality and properties of the prospective ESKs.

Our approach to ESKs is different. Wojdel and Íñiguez [10] showed that the common  $180^\circ$  domain walls (DWs) of  $\text{PbTiO}_3$  (PTO) have a Bloch-like character at low temperatures, with a spontaneous electric polarization confined within the DW plane (Figs. 1c and 1d). Simulations further predict that such Bloch DWs occur in the PTO layers of PTO/STO superlattices, and cause them to be chiral, which explains recent experimental observations [23]. Here we show how these Bloch DWs also allow us to create ESKs with tunable and unique properties.

In view of Fig. 1d, consider the situation in Fig. 1e, where a columnar nano-domain (ND) is embedded in a big matrix of opposite polarization, and the corresponding nano domain wall (NDW) forms a closed surface. We run second-principles simulations of NDs like that in Fig. 1e, starting from a configuration where all electric dipoles align strictly along  $-z$  (matrix) or  $+z$  (ND), and relaxing the structure using the model potential previously applied to PTO [9, 10] and PTO/STO [18, 23, 24]. Figure 2a shows the lowest-energy solution thus obtained, which features a Bloch-like NDW. Figure 2d shows the corresponding  $q(x, y)$ , which presents local maxima at the NDW corners and a total topological charge  $Q = 1$ . The simulated ND is thus an electric skyrmion. In the Supplementary Note 1 and Fig. 1, we discuss in some detail how this ESK fits the classification schemes in the MSK literature.

Figure 2 shows results for a square ND with a small section of about  $6 \times 6$  perovskite cells ( $\sim 2.3^2 \text{ nm}^2$ ); yet, as shown in Supplementary Fig. 2, the predicted ESK is robust upon variations of the shape and size of the ND, and could be made much bigger. Likewise, the ESK can be as small as the smallest stable ND; this suggests the possibility of reaching ESK radii of a few nm, well beyond what is typical for MSKs. (Very small MSKs have been reported, though [2, 25].)

Monte Carlo simulations (Fig. 2g) indicate that the

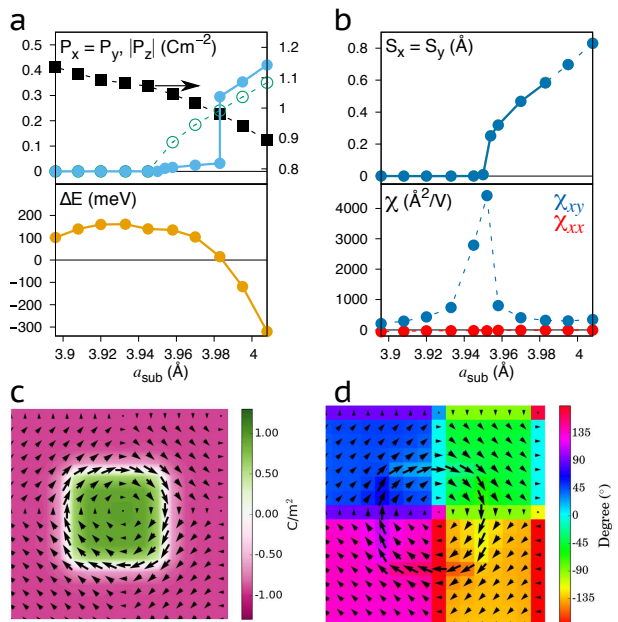


FIG. 3. Panel (a): Polarization (top) and energy difference between the NDW-polar and ND-ESK states (bottom) as a function of the epitaxial constraint  $a_{\text{sub}}$ ; details as in Fig. 2. Panel (b): position of the ESK center (top) and related susceptibility (bottom) as a function of  $a_{\text{sub}}$  (see text for definitions). In the top figure, the dashed line marks the regime where the polar-NDW becomes the ground state and the polar ESK is a metastable solution. Panel (c): polarization map for the polar ESK state that appears for  $a_{\text{sub}} \gtrsim 3.95 \text{ \AA}$ . Panel (d): for the same state, color map for the orientation of the in-plane polarization ( $P_x, P_y$ ), evidencing the formation of  $90^\circ$  DWs.

electric dipoles at the NDW disorder upon heating, yielding a topological transition between skyrmionic ( $Q = 1$ ) and normal ( $Q = 0$ ) ND states at  $T_Q \sim 235 \text{ K}$ .

We now consider the response of our ESK to applied in-plane electric fields (Fig. 2h). We can distinguish two regimes. For moderate fields we find a seemingly-trivial linear dielectric behavior. Yet, the reaction of the ESK (Figs. 2b and 2e) is peculiar: for a field applied along  $(1, 1)$ , the ESK center moves along the perpendicular  $(1, \bar{1})$ , which is reminiscent of the response to fields and currents observed in some MSKs [2].

For larger fields, the ESK undergoes a discontinuous topological transition (Figs. 2h and 2i) to a state with  $Q = 0$  in which the NDW becomes polarized in-plane (Figs. 2c and 2f). Further simulations show that this NDW-polar state is metastable at zero field, with a dipole moment of about  $1.4 \times 10^{-28} \text{ C m}$ , and an energy about  $6.7 \text{ meV}$  per DW cell above the ESK ground state. Note that our ESK behaves as an antiferroelectric [26].

Let us now consider the effect of epitaxial strain, which can be imposed by growing films on suitable substrates, and is known to tune the properties of FE perovskites [27]. For example, if we start with a PTO film in a  $z$ -polarized monodomain state, and apply a tensile strain

in the  $xy$  plane, the polarization will eventually rotate by developing  $P_x = P_y$  components. To test whether such a perturbation affects our ESK, we run simulations imposing a square substrate with lattice constants  $a_{\text{sub}} = b_{\text{sub}}$ . Our results are summarized in Fig. 3.

For  $a_{\text{sub}}$  close to the theoretical bulk value ( $a_{\text{bulk}} = 3.93 \text{ \AA}$ ), the ESK remains essentially identical to the solution presented above in bulk-like conditions (i.e., with no elastic constraint). The surprises commence for larger  $a_{\text{sub}}$  values. As shown in Fig. 3a,  $a_{\text{sub}} \approx 3.95 \text{ \AA}$  marks the onset of the said polarization rotation, in both the monodomain and ND-ESK cases; yet, the  $P_x = P_y$  components are smaller when the ESK is present. Figures 3c and 3d show representative results in this regime: locally, the electric dipoles develop an in-plane component, but they form  $90^\circ$  domains that are compatible with the ESK topology, yielding a  $Q = 1$  multi-domain structure with nearly null in-plane polarization. In fact, the small  $P_x = P_y$  values obtained in the ESK case for  $a_{\text{sub}} \gtrsim 3.95 \text{ \AA}$  are mainly due to a symmetry breaking affecting the skyrmion itself: the ESK center moves away from the midpoint of the ND, thus developing an in-plane polarization. This polar ESK is very similar to the one obtained above (Fig. 2b) by applying a field to the (high-symmetry, non-polar) skyrmion. Epitaxial strain allows us to stabilize the polar ESK state in absence of electric field.

To better characterize the transition at  $a_{\text{sub}} \approx 3.95 \text{ \AA}$ , we define the position of the ESK center as [28]

$$S_\alpha = \frac{1}{Q} \int r_\alpha q(x, y) dx dy, \quad (3)$$

where  $\alpha = x, y$ ;  $r_x = x$  and  $r_y = y$ . We also introduce the susceptibility

$$\chi_{\alpha\beta} = \frac{\partial S_\alpha}{\partial E_\beta}, \quad (4)$$

where  $E_\beta$  is the  $\beta$  component of an applied electric field. As shown in Fig. 3b, this susceptibility nearly diverges at the skyrmion-skyrmion transition, which reflects its second-order character and the very soft (low-energy) vibrations of the ESK center. Accordingly, as shown in Supplementary Fig. 3, for  $a_{\text{sub}} \gtrsim 3.95 \text{ \AA}$ , we have a region in which moderate fields can be used to switch the polar ESK among its four symmetry-equivalent states, suggesting a novel possibility for storing information.

Finally, for  $a_{\text{sub}} \approx 3.98 \text{ \AA}$  we observe a first-order topological transformation to a normal ( $Q = 0$ ) state that is strongly polar. This solution is all but identical to the NDW-polar state discussed above, obtained under relatively large in-plane electric fields (Figs. 2c and 2f). By favoring the occurrence of in-plane dipoles, the tensile strain reverses the relative stability of the ESK and NDW-polar configurations, yielding the latter as the ground state even with no electric field applied.

In sum, our results show that, by writing columnar ferroelectric domains within a matrix of opposite polarization, one can stabilize electric skyrmions thanks

to the Bloch-like structure of the domain walls. These skyrmions resemble the soft bubbles of some magnetic materials [1], and have an analogous origin, albeit important differences (electric dipoles can vanish, so it is not obvious a bubble domain will yield a skyrmion). The predicted skyrmions show the expected topological properties and some novel ones, including various iso-topological and topological transitions. For our skyrmions to move, one should seek conditions favoring domain-wall mobility, as e.g. in the “domain liquid” of Ref. 18. With plenty of challenges and opportunities ahead, this work propels the field of electric skyrmions.

**Acknowledgements.** This work is mainly funded by the Luxembourg National Research Fund through the CORE program (Grant FNR/C15/MS/10458889 NEWALLS, M.A.P.G. and J.Í.). C.E.S. is supported by an FNR-AFR Grant No. 9934186. P.G.F. and J.J. acknowledge financial support from the Spanish Ministry of Economy and Competitiveness through grant No. FIS2015-64886-C5-2-P. P.G.F. is also funded by the “Ramón y Cajal” grant No. RyC-2013-12515.

**Author Contributions.** Work conceived by M.A.P.G. and J.Í., and executed by M.A.P.G. with the supervision of J.J. and J.Í. and contributions from C.E.S. and P.G.F. All authors discussed the results. The manuscript was prepared by M.A.P.G. and J.Í. with contributions from all authors.

## Methods

For the second-principles simulations we use the same methodology and potentials described in previous works [9, 10], as implemented in the SCALE-UP package [9, 29]. The employed PTO potential was fitted to density functional theory results within the local density approximation (LDA) [30, 31] and inherits LDA’s well-known overbinding problem; thus, as customarily done in these cases [9, 32], we include an expansive hydrostatic pressure (−13.9 GPa) to compensate for it. The resulting potential yields a qualitatively correct description of the lattice-dynamical properties and structural phase transitions of PTO; further, it has been explicitly checked

against direct first-principles simulations in what regards the Bloch-type structure of PTO’s 180° DWs [10], a result critically important for the present work.

To solve the models we use standard Monte Carlo and Langevin molecular-dynamics methods. Typically, we run simulated-annealing calculations to perform structural relaxations, and Metropolis Monte Carlo to compute thermal averages. For the former, we typically work with periodically-repeated supercells made of  $16 \times 16 \times 1$  elemental 5-atom cells (i.e., 1,280 atoms), our ND being formed by approximately  $6 \times 6 \times 1$  cells. For the latter, we work with a  $16 \times 16 \times 10$  supercell (i.e., 12,800 atoms) with an embedded  $6 \times 6 \times 10$  ND; at a given temperature, we typically run 20,000 sweeps for thermalization, followed by 20,000 (100,000 around  $T_Q$ ) additional sweeps to compute averages.

We compute local polarizations within a linear approximation, using the atomic displacements from the (cubic) reference perovskite structure and the corresponding Born charge tensors. We compute the topological charge  $Q$  by (1) processing our local dipoles to obtain a normalized polarization field ( $|\mathbf{u}(x, y)| = 1$ ) and (2) applying the scheme in Ref. 33; we find this yields well converged results even for our rapidly changing polarization fields. To compute the probability distribution for  $Q$  from our Monte Carlo runs, we work with polarization maps  $\mathbf{u}(x, y)$ , an associated topological densities  $q(x, y)$ , corresponding to  $16 \times 16 \times 1$  slices of our  $16 \times 16 \times 10$  supercell.

Note that, typically, a given  $\mathbf{u}(x, y)$  map can be viewed as a linear superposition of modes with different characteristic topology. For example, around  $T_Q$ , the system is characterized by fluctuations that resemble the ESK ( $Q = 1$ ) and polar ( $Q = 0$ ) solutions discussed in our manuscript, which constitute its lowest-energy excitations. Yet, it is important to realize that  $Q$  is not linear in  $\mathbf{u}(x, y)$ ; in fact, for any given state, even if the structure is the result of a superposition of vibrational modes, our calculation procedure [33] yields an integer  $Q$  corresponding to the dominant mode, instead of a linear combination of  $Q$ ’s. Hence, the corresponding probability distribution pertains only to interger  $Q$  values.

- 
- [1] Seki, S. & Mochizuki, M. *Skyrmions in Magnetic Materials*. SpringerBriefs in Physics (Springer International Publishing, Cham, 2016).
  - [2] Nagaosa, N. & Tokura, Y. Topological properties and dynamics of magnetic skyrmions. *Nature Nanotechnology* **8**, 8579–8589 (2013).
  - [3] Kang, W., Huang, Y., Zhang, X., Zhou, Y. & Zhao, W. Skyrmion-electronics: An overview and outlook. *Proceedings of the IEEE* **104**, 2040–2061 (2016).
  - [4] Fert, A., Reyren, N. & Cros, V. Magnetic skyrmions: advances in physics and potential applications. *Nature Reviews Materials* **2**, 17031 (2017).
  - [5] Röbber, U. K., Bogdanov, A. N. & Pfleiderer, C. Spontaneous skyrmion ground states in magnetic metals. *Nature* **442**, 797 (2006).
  - [6] Naumov, I. I., Bellaiche, L. & Fu, H. Unusual phase transitions in ferroelectric nanodisks and nanorods. *Nature* **432**, 737–740 (2004).
  - [7] Nahas, Y. *et al.* Discovery of stable skyrmionic state in ferroelectric nanocomposites. *Nature Communications* **6**, 8542 (2015).
  - [8] Yadav, A. K. *et al.* Observation of polar vortices in oxide superlattices. *Nature* **530**, 198–201 (2016).
  - [9] Wojdeł, J. C., Hermet, P., Ljungberg, M. P., Ghosez, P. & Íñiguez, J. First-principles model potentials for lattice-dynamical studies: general methodology and example of application to ferroic perovskite oxides. *Journal*

- of Physics: Condensed Matter* **25**, 305401 (2013).
- [10] Wojdel, J. C. & Íñiguez, J. Ferroelectric transitions at ferroelectric domain walls found from first principles. *Physical Review Letters* **112**, 247603 (2014).
- [11] Tomasello, R. *et al.* A strategy for the design of skyrmion racetrack memories. *Scientific Reports* **4**, 6784 (2014).
- [12] Parkin, S., Hayashi, M. & Thomas, L. Magnetic domain-wall racetrack memory. *Science* **320**, 190–4 (2008).
- [13] Lines, M. E. & Glass, A. M. *Principles and Applications of Ferroelectrics and Related Materials*. Oxford Classic Texts in the Physical Sciences (Clarendon Press, Oxford, 1977).
- [14] Rabe, K. M., Ahn, C. H. & Triscone, J. (eds.) (Springer Berlin Heidelberg, Berlin, Heidelberg, 2007).
- [15] Dawber, M., Gruverman, A. & Scott, J. F. Skyrmion model of nano-domain nucleation in ferroelectrics and ferromagnets. *Journal of Physics: Condensed Matter* **18**, L71 (2006).
- [16] Chen, W. J. *et al.* Mechanical switching in ferroelectrics by shear stress and its implications on charged domain wall generation and vortex memory devices. *RSC Advances* **8**, 4434–4444 (2018).
- [17] Li, L. *et al.* Defect-induced hedgehog polarization states in multiferroics. *Physical Review Letters* **120**, 137602 (2018).
- [18] Zubko, P. *et al.* Negative capacitance in multidomain ferroelectric superlattices. *Nature* **534**, 524–528 (2016).
- [19] Aguado-Puente, P. & Junquera, J. Structural and energetic properties of domains in  $\text{PbTiO}_3/\text{SrTiO}_3$  superlattices from first principles. *Physical Review B* **85**, 184105 (2012).
- [20] Zubko, P., Stucki, N., Lichtensteiger, C. & Triscone, J. M. X-Ray Diffraction Studies of  $180^\circ$  Ferroelectric Domains in  $\text{PbTiO}_3/\text{SrTiO}_3$  Superlattices under an Applied Electric Field. *Physical Review Letters* **104**, 187601 (2010).
- [21] Zhang, Q. *et al.* Nanoscale bubble domains and topological transitions in ultrathin ferroelectric films. *Advanced Materials* **1702375** (2017).
- [22] Louis, L., Kornev, I., Geneste, G., Dkhil, B. & Bellaiche, L. Novel complex phenomena in ferroelectric nanocomposites. *Journal of Physics: Condensed Matter* **24**, 402201 (2012).
- [23] Shafer, P. *et al.* Emergent chirality in the electric polarization texture of titanate superlattices. *Proceedings of the National Academy of Sciences* **115**, 915–920 (2018).
- [24] Damodaran, A. R. *et al.* Phase coexistence and electric-field control of toroidal order in oxide superlattices. *Nature Materials* **16**, 1003–1009 (2017).
- [25] Romming, N., Kubetzka, A., Hanneken, C., von Bergmann, K. & Wiesendanger, R. Field-dependent size and shape of single magnetic skyrmions. *Physical Review Letters* **114**, 177203 (2015).
- [26] Rabe, K. M. Antiferroelectricity in oxides: A reexamination. In *Functional Metal Oxides*, chap. 7, 221–244 (Wiley-Blackwell, 2013).
- [27] Schlom, D. G. *et al.* Strain tuning of ferroelectric thin films. *Annual Review of Materials Research* **37**, 589 (2007).
- [28] Papanicolaou, N. & Tomaras, T. Dynamics of magnetic vortices. *Nuclear Physics B* **360**, 425 – 462 (1991).
- [29] García-Fernández, P., Wojdel, J. C., Junquera, J. & Íñiguez, J. Second-principles method for materials simulations including electron and lattice degrees of freedom. *Physical Review B* **93**, 195137 (2016).
- [30] Hohenberg, P. & Kohn, W. Inhomogeneous electron gas. *Physical Review* **136**, B864 (1964).
- [31] Kohn, W. & Sham, L. J. Self-consistent equations including exchange and correlation effects. *Physical Review* **140**, A1133 (1965).
- [32] Zhong, W., Vanderbilt, D. & Rabe, K. M. Phase transitions in  $\text{BaTiO}_3$  from first principles. *Physical Review Letters* **73**, 1861 (1994).
- [33] Berg, B. & Lüscher, M. Definition and statistical distributions of a topological number in the lattice  $O(3)$   $\sigma$ -model. *Nuclear Physics B* **190**, 412 – 424 (1981).